



Advancements in Computer-Generated Holographic Communication: A Comprehensive Comparative Study of Holographic Algorithms for Enhanced Security in Communication Systems

Md. Rakib Hossain^{1*}, S M Abdur Razzak².

¹*Dept. of Electronics & Telecommunication Engineering, Rajshahi University of Engineering & Technology (RUET), Rajshahi, Bangladesh.*

²*Dept. of Electrical & Electronic Engineering, Rajshahi University of Engineering & Technology (RUET), Rajshahi, Bangladesh.*

ARTICLE INFORMATION

Received date: 3rd Apr 2024
 Revised date: 5th Nov 2024
 Accepted date: 14th Nov 2024

Keywords

CGH,
 Fraunhofer Algorithm
 GS Algorithm
 Advanced Fresnel Algorithm
 HCS
 FCG

ABSTRACT

This study investigates the utilization of computer-generated holograms (CGH) in secure communication systems, employing three advanced algorithms: Fraunhofer, Gerchberg-Saxton (GS), and Fresnel. At the transmitter, digital holograms of the main and reference objects are generated and combined for transmission. At the receiver, these holograms are separated to reconstruct the main object image. The Fraunhofer algorithm generates holograms by combining far-field amplitudes but suffers from image overlapping issues, while the GS algorithm iteratively enhances phase retrieval but the procedure is not so fast. On the other hand, The Fresnel algorithm utilizes Fast Fourier Transform for hologram calculation. However, the proposed advanced Fresnel Fourier hologram method demonstrates promising results for efficient transmission and reception due to its fast processing and high-quality reconstruction with an entropy of 7.9895, redundancy of 0.0105, and RMSE of 0.84, outperforming Fraunhofer's entropy of 7.4232 and RMSE of 1.02, as well as GS's redundancy of 0.0120 and RMSE of 0.72. This study shows the most uniform pixel distribution and lower correlation between adjacent pixels and sets the stage for the practical implementation of secure communicative CGH systems, offering enhanced security in communication through nearly impossible decoding of transmitted holograms without reference information. The study also emphasizes the significance of iterative techniques like Gerchberg-Saxton (GS) for enhancing phase retrieval accuracy in addition to addressing image overlapping issues. Furthermore, subsequent investigations could focus on real-world applications and developments in CGH technology to address changing requirements in secure communication networks.

1. Introduction

Holography revolutionizes 3D imaging by capturing and reconstructing light's intensity and phase, unlike traditional photography, which lacks depth and perspective [1]-[3]. It involves two stages: recording interference patterns using coherent light beams and reconstructing 3D images by illuminating holograms with coherent light [4]-[6], as shown in Figure 1.

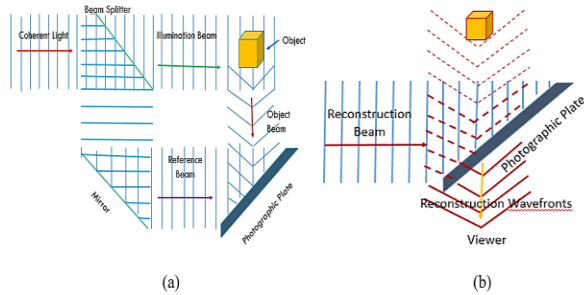


Figure 1. (a) Recording and (b) Reconstruction of hologram.

Digital holography extends traditional methods to applications like data storage, microscopy, and secure communication [7]-[9]. Computer-Generated Holography (CGH) creates holograms numerically, eliminating physical objects [10]. CGH enables the generation of amplitude, phase, rainbow, transmission, and reflection holograms, with advanced Fresnel holograms offering lensless 3D reconstruction [2], [11], [12]. Challenges in computation speed and image quality are addressed by advancements in Fourier-based methods and efficient algorithms [13], [14].

Computer-Generated Holography (CGH) uses numerical methods to create holograms, bypassing optical processes [15]. Key contributions include Gabor's foundational work and Denisyuk's 3D reflections [16]. CGH relies on factors like light source and design, with computational techniques enhancing traditional interference pattern recording [17], [18]. Advances in color CGH improve 3D displays by reducing noise and enhancing image quality. Faster calculations, hardware optimization, and iterative algorithms enhance advanced Fresnel holography, while micro/nano-fabrication strengthens holographic security [3]-[7], [17]. This research develops advanced CGH algorithms to improve imaging and efficiency, addressing current challenges and supporting secure communication systems [18].

2. Research Methodology

(i) Fraunhofer Holographic Algorithm

The main steps for Fraunhofer hologram, involved in CGH development and object reconstruction are outlined in Figure 2.

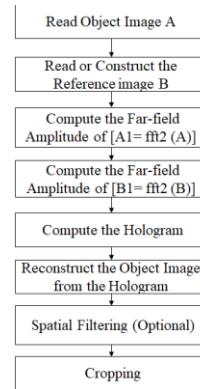


Figure 2. Algorithm for Fraunhofer hologram.

Object and reference sizes are chosen to match PC speed. The object wave is created using simple shapes or loaded images, followed by generating a reference wave (e.g., plane wave). Hologram creation combines object and reference matrices, calculates intensity, and applies filtering. The filtered hologram undergoes Fourier Transform, producing the image intensity matrix. Fraunhofer diffraction may show two object versions, one inverted. Cropping reveals larger holograms yield closer matches to the original image.

(ii) Gerchberg-Saxton (GS) Holographic Algorithm

The GS algorithm retrieves phase information using intensity measurements from two planes related by a Fourier Transform. In this process, the unshaped light beam's depth distribution, I_H and the target intensity distribution, I_T in the Fourier plane are stored as 2D real-valued arrays.

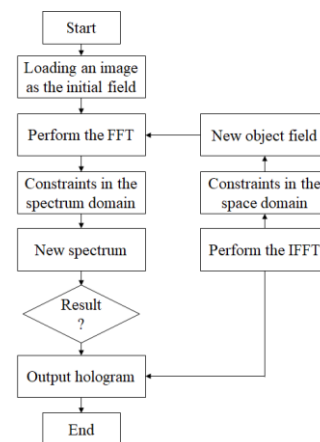


Figure 3. Algorithm for GS hologram.

The light fields in the hologram and Fourier planes are represented as 2D complex arrays, u_n and u'_n , with n indicating the iteration number.

$$q(x, y) = \frac{z}{j\lambda} \iint_{\infty} f(x, y) \frac{1}{r^2} \exp(jkr) d\xi dn$$

where, $r = \sqrt{z^2 + (x - \xi)^2 + (y - n)^2}$

$$= z \sqrt{1 + \frac{(x-\xi)^2 + (y-n)^2}{z^2}}$$

$$= z + \frac{(x-\xi)^2 + (y-n)^2}{2z} - \frac{[(x-\xi)^2 + (y-n)^2]^2}{8z^3} \quad (1)$$

The phase distribution in the hologram plane, φ_n^H , is initially uniform or arbitrary. The GS algorithm iteratively improves this phase distribution. Using the previous phase φ_{n-1}^H , the target plane phase φ_n^T , is computed via Eq. (4) after obtaining the initial field with Eq. (3) through FFT. Combining φ_n^T with target intensity I_T , using Eq. (5) yields the field u_n^T , and Eq. (6) recalculates φ_n^H . This process facilitates holographic light shaping and optical simulations using Fourier Transforms, as shown in Figure 3.

$$i. e. \varphi_0^H \equiv 0 \quad (2)$$

$$u_n^H = \sqrt{I_H} \exp(i\varphi_{n-1}^H) \quad (3)$$

$$\varphi_n^T = \arg(FFT(u_n^H)) \quad (4)$$

$$u_n^T = \sqrt{I_T} \exp(i\varphi_n^T) \quad (5)$$

$$\varphi_n^H = \arg(FFT^{-1}(u_n^T)) \quad (6)$$

(iii) Advanced Fresnel Holographic Algorithm

In Fresnel holography, the object pattern's complex field is obtained via a Fourier Transform (FT), and a tilted plane-wave reference light creates the hologram, which can be depicted in Figure 4.

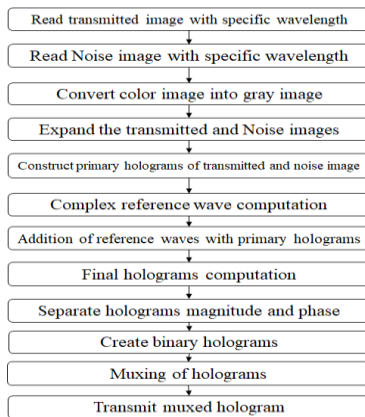


Figure 4. Algorithm for Advanced Fresnel hologram.

The formula models beam propagation, predicting intensity and phase, separating amplitude and phase in 2D or 3D apertures for secure holographic systems. Moreover, scalar diffraction theory defines spherical

wavefronts, with object and reference beams creating interference patterns through the Fresnel-Kirchhoff integral:

$$R(\xi', \eta') = \frac{i}{\lambda} \int_{-\infty}^{\infty} \int_{-\infty}^{\infty} h(x, y) E_R(x, y) \frac{\exp(-i\frac{2\pi}{\lambda}\rho)}{\rho} dx dy \quad (7)$$

$$\text{with, } \rho = \sqrt{(\xi' - x)^2 + (\eta' - y)^2 + d^2} \quad (8)$$

Here, the coordinates of Eq. (7) and Eq. (8) are displayed in Figure 5, where the functions of the reconstructed image, hologram, object image, reference or noise image, and hologram are, respectively, $R(\xi', \eta')$, $h(x, y)$, $O(\xi, \eta)$, and $E_R(x, y)$. In this case, ρ is the distance between two corresponding points in two adjacent planes, μ is the wavelength, and d is the distance between two adjacent planes. The reconstructed image $R(\xi', \eta')$ can be acquired through either the convolution or Fresnel methods. From the hologram function $h(x, y)$, the object image can be recreated using either method.

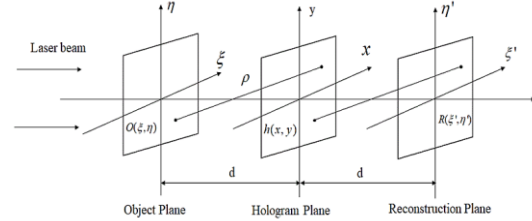


Figure 5. Coordinate system.

The left and right portions of Figure 6 show identical processes for creating and reconstructing a hologram, with the hologram function derived by modifying variables in Eq. (7).

$$h(x, y) = \frac{i}{\lambda} \int_{-\infty}^{\infty} \int_{-\infty}^{\infty} O(\xi, \eta) E_R(\xi, \eta) \frac{\exp(-i\frac{2\pi}{\lambda}\rho)}{\rho} d\xi d\eta \quad (9)$$

Since the form of Eq. (9) is the same as that of Eq. (7), the hologram function $h(x, y)$ can be obtained from the object function $O(\xi, \eta)$ using the Fresnel or convolution methods as well. Eq. (8) is expanded to a Taylor series by the Fresnel approximation, which ignores high-order terms. Eq. (8) is then recast as follows:

$$\rho = d + \frac{(\xi - x)^2}{2d} + \frac{(\eta - y)^2}{2d}$$

$$= d + \frac{(\xi - x)^2 + (\eta - y)^2}{2d} \quad (10)$$

Replacing the numerator by Eq. (10) and the denominator by d because x, y, ξ and η values are small compared to the object distance d , then the Eq. (9) becomes:

$$\begin{aligned}
 & h(x, y) \\
 &= \frac{i}{\lambda d} \exp(-i \frac{2\pi}{\lambda} d) \exp[-i \frac{\pi}{\lambda d} (x^2 \\
 &+ y^2)] \cdot \int_{-\infty}^{\infty} \int_{-\infty}^{\infty} O(\xi, \eta) E_R(\xi, \eta) \exp[-i \frac{\pi}{\lambda d} (\xi^2 \\
 &+ \eta^2)] \cdot \exp[-i \frac{2\pi}{\lambda d} (x\xi + y\eta)] d\xi d\eta \quad (11)
 \end{aligned}$$

In order to digitize Eq. (11), we present the subsequent substitution:

$$v = \frac{x}{\lambda d}; u = \frac{y}{\lambda d} \quad (12)$$

The reference function $E_R(x, y)$ is a unit matrix and the integral part of Eq. (11) can be expressed using a Fourier Transform (FT). Combining Eq. (11) and (12) results in:

$$h(u, v) = \frac{i}{\lambda d} \exp(i \frac{2\pi}{\lambda d} d) \exp[-i \pi d (v^2 + u^2)] \times F^{-1}\{O(\xi, \eta) \exp[-i \frac{\pi}{\lambda d} (\xi^2 + \eta^2)]\} \quad (13)$$

Where $F^{-1}\{\}$ is an Inverse Fourier Transform (IFT). Eq. (13), which applies the advanced Fresnel method to the generation of CGH. The hologram function $h(x, y)$, which corresponds to the same object image function $O(\xi, \eta)$, can be obtained using this equation. Eq. (9) can be replaced with Eq. (11) to produce the following superposition integral:

$$h(x, y) = \int_{-\infty}^{\infty} \int_{-\infty}^{\infty} O(\xi, \eta) g(\xi, \eta, x, y) dx dy \quad (14)$$

$$g(\xi, \eta, x, y) = \frac{i \exp[-i \frac{2\pi}{\lambda} \sqrt{(d^2 + (\xi-x)^2 + (\eta-y)^2)}]}{\lambda \sqrt{(d^2 + (\xi-x)^2 + (\eta-y)^2)}} \quad (15)$$

This superposition integral regarded as a convolution. So, Eq. (14) becomes:

$$F^{-1} \left\{ F[O(\xi, \eta)] F \left[\frac{i \exp[-i \frac{2\pi}{\lambda} \sqrt{(d^2 + (\xi-x)^2 + (\eta-y)^2)}]}{\lambda \sqrt{(d^2 + (\xi-x)^2 + (\eta-y)^2)}} \right] \right\} \quad (16)$$

Where $F[\]$ is a Fourier Transform.

Digital holograms enable 3D correlation by capturing different perspectives of a 3D object. The correlation coefficient between a target 3D perspective and a reference object's perspective is expressed as:

$$C(x, y) = \mathfrak{F}^{-1} \{ \mathfrak{F}^\eta \{ H_{tar}(x, y; z; \alpha, \beta) \} \{ \xi^\eta \{ H_{ref}(x, y; z; \alpha', \beta') \} \} \} \quad (17)$$

$\mathfrak{F}^\eta, \mathfrak{F}^{-1}$ are the FT with order η and IFT, respectively. $H(x, y; z; \alpha, \beta)$ represents a part of the hologram used for reconstructing an angular view (α, β) of a 3D

object an $H_{ref}(x, y; z; \alpha', \beta')$ represent a perspective of the target object and the given perspective of reference object, respectively.

3. Experimental Results Analysis

In this section, the result analysis of the three different algorithms: Fraunhofer, GS, and Advanced Fresnel have been discussed through different parameters.

(i) Result Analysis of Fraunhofer Holographic Algorithm

The result analysis of Fraunhofer algorithm can be divided into two main parts. One is the Transmitter Side Analysis and other is the reconstructed image and receiver side analysis

Transmitter Side Analysis

The transmitter adds far-field matrices of the main and reference images, calculating hologram intensity as the square of the matrix. MATLAB simulations include transmitter, receiver, and color reproduction steps. Figure 6 shows (a) the main object, (b) its gray image, (c) the reference image, and (d) its hologram for muxing.

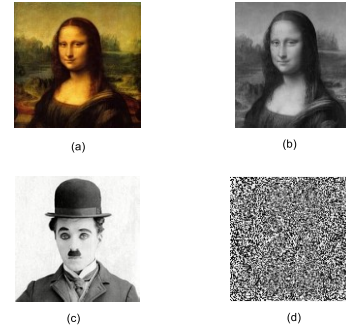


Figure 6. Generation and transmission of hologram (a) Object image, (b) Gray image, (c) Reference image, (d) Computer Generated hologram.

Reconstructed Image and Receiver Side Analysis

The receiver generates the reconstructed gray image from the hologram, but a "Ringing Effect" may cause a double image. Figure 7 (a) shows the received hologram, and Figure 7 (b) displays its reconstructed image.

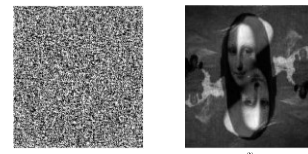


Figure 7. Reconstruction of hologram (a) Received Hologram, (b) Reconstructed gray image.

(ii) Result Analysis of GS Holographic Algorithm

The GS algorithm tackles phase retrieval using amplitude data at two Fourier-related planes, focusing on hologram generation, reconstruction, and performance analysis of the gray main image.

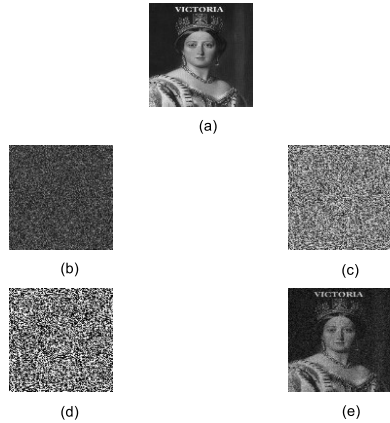


Figure 8. (a) Original object, (b) random-phase mask with phase ranging from $(-\pi$ to $\pi)$, (c) and (d) spectrum of the object with the random-phase mask, and (e) reconstructed image from the hologram.

Figure 8 shows the original object (a), a random-phase mask (b), and their spectra (c). Despite uniform modulus assumptions, the reconstructed CGH (d) shows speckle noise, which optimization techniques like the GS algorithm reduce, improving image quality.

Transmitter Side Analysis

In this work, the primary image is encrypted using a noise image. Both are encoded as holograms for secure communication and then converted into binary holograms. These binary holograms are combined via muxing, as shown in Figure 9 and 10.

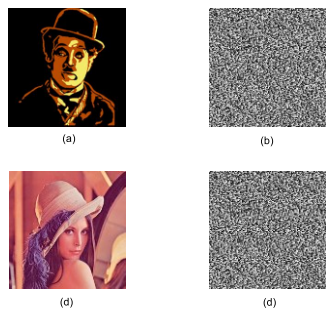


Figure 9. Phase mask hologram (a) Main object image, (b) Hologram of main object image, (c) Noise image, (d) Hologram of noise image.

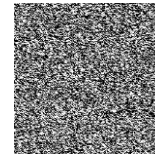


Figure 10. Muxed Hologram.

Receiver Side Analysis

The transmitted hologram was demuxed at the receiver using the reference object image, yielding the primary grayscale object image and then converted the gray object image into color image which is shown in Figure 11. However, Figure 12 shows reduced error and RMSE with increased iterations where, comparing target and reconstructed images with varying iterations (n) and pixel count (s).



Figure 11. Received GS hologram (a) Demuxed hologram, (b) Reconstructed gray image, (c) Reconstructed color image.



Figure 12. Reconstruct the received image in various iteration.

RMSE is used to evaluate hologram reconstruction quality and is defined as:

$$RMSE = \sqrt{\frac{1}{MN} \sum [|\psi(m, n)| - A(m, n)]^2} \quad (18)$$

Where A (m, n) is the target image, ψ (m, n) is the original image, (m, n) are the sampling indices, and M and N are the sampling numbers along the x-axis and y-axis, respectively. For this test, it can be concluded that the majority of reconstruction improvement occurs during the first 100 iterations, after which the RMSE from Eq. (18) is computed. Moreover, the contrast in a given image is:

$$\text{Contrast} = \frac{I_{max} - I_{min}}{I_{max} + I_{min}} \quad (19)$$

where I_{max} and I_{min} represent the intensity image's maximum and minimum values, respectively, across all pixels.

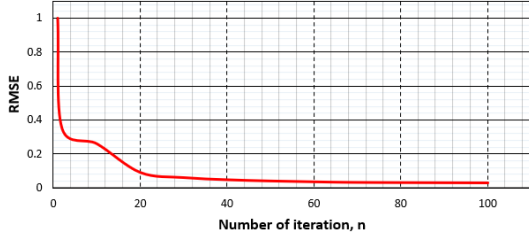


Figure 13. RMSE between the reconstructed image and the target image, as a function of the number of iterations.

Performance Analysis of the GS Algorithm

To the validation quality of the GS algorithm, three performance parameters are discussed in this section and they are: Histogram analysis, Correlation coefficient analysis and Entropy analysis.

Histogram Analysis

The histogram shows pixel distribution, with uniformity preventing plain-text attacks. Figure 14 illustrates the hologram's pixel values are evenly spread, safeguarding against information leakage.

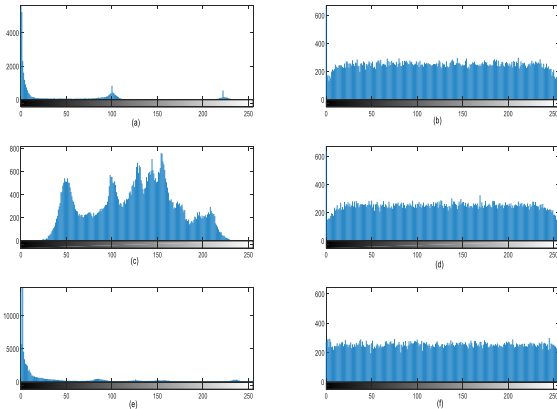


Figure 14. Histogram of (a) Main object image, (b) main object image hologram, (c) ref. image, (d) ref. image hologram, (e) reconstructed image, (f) transmitted image hologram.

Correlation Coefficient Analysis

The hologram quality is measured by the correlation coefficient between adjacent pixels of the encrypted image by following equations.

$$\gamma = \frac{\text{Conv}(x, y)}{\sqrt{D(x)D(y)}} \quad (20)$$

$$D(x) = \frac{1}{M} \sum_{i=1}^M (x - \bar{x})^2 \quad (21)$$

$$\text{Conv}(x, y) = \frac{1}{M} \sum_{i=1}^M (x - \bar{x})(y - \bar{y}) \quad (22)$$

Where M is the number of randomized pairs and x, y are pixel values. Table 1 shows the correlation coefficient from the proposed method, demonstrating effective pixel randomization. The original image has high pixel correlation, but after hologram generation, pixel values are uniformly distributed, enhancing security.

Table 1. Correlation Coefficient Analysis of Hologram

| <i>Correlation Coefficient of Hologram</i> | | |
|--|-----------------|-------------------|
| <i>Image</i> | <i>Position</i> | |
| | <i>Vertical</i> | <i>Horizontal</i> |
| Main object image | 0.9170 | 0.9637 |
| Hologram of main object image | 0.3877 | 0.1899 |
| Reference image | 0.9072 | 0.9699 |
| Hologram of reference image | 0.0049 | 0.0007 |
| Muxed hologram | -0.0006 | 0.0052 |
| Reconstructed image | 0.9512 | 0.9663 |

Entropy Analysis

The histogram shows a uniform distribution of hologram pixels. Information entropy, which measures signal randomness, is calculated using the equation:

$$H(s) = - \sum_{i=0}^{N-1} P(S_i) \log_2 P(S_i) \quad (23)$$

Where the entropy is given in bits and $P(S_i)$ denotes the probability of symbol S_i . The optimal entropy for a message source S is represented by $H(S) = 8$, which corresponds to a true random source and is achieved by an ideal source S emitting 256 symbols with equal probability, i.e. $S = \{s_1, s_2, \dots, s_{256}\}$. The GS algorithm produces entropy values near 8, as shown in Table 2, ensuring strong security. An 8-bit, 256×256 image was used to improve output entropy, making the GS algorithm ideal for practical communication system applications.

Table 2. Entropy Analysis of Hologram

| <i>Information Entropy Analysis of hologram</i> | |
|---|----------------|
| <i>Image</i> | <i>Entropy</i> |
| Main object image | 3.1980 |
| Hologram of main object image | 7.9469 |
| Reference image | 7.4471 |
| Hologram of reference image | 7.9487 |
| Muxed hologram | 7.9887 |
| Reconstructed image | 4.0849 |

iii) Result Analysis of Advanced Fresnel Holographic Algorithm

Transmitter Side Analysis

The transmitter side analysis includes Fresnel Hologram a) Transmitted main object image, b) Converted grayscale version of object image, and c) Hologram of main object image which is depicted in Figure 15. On the contrary, the reference image, grayscale version of reference image and hologram of reference image and Transmitted Hologram are depicted in Figure 16 (a), (b), (c) and Figure 17.

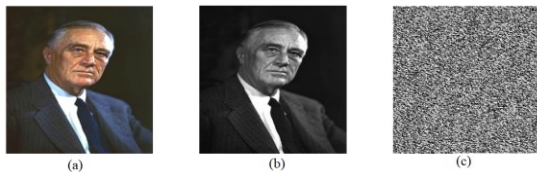


Figure 15. Fresnel hologram (a) Transmitted main object image, (b) Converted grayscale version of object image, (c) Hologram of main object image.

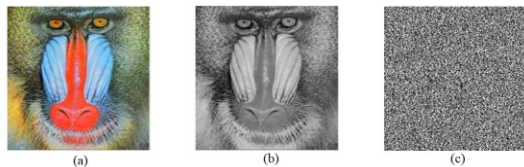


Figure 16. (a) Reference image, (b) Converted grayscale version of reference image, (c) Hologram of reference image.

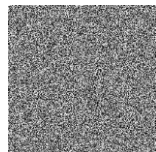


Figure 17. Transmitted Hologram

The advanced Fresnel Fourier Algorithm processes a 256×256 image of Franklin D. Roosevelt and a reference "Mandrill" image, with histogram analysis. The algorithm encodes the noise image's hologram for secure transmission. The transmitted hologram is

created by combining reference waves and primary holograms, with magnitude and phase stored separately for secure FCGH communication.

Receiver Side Analysis

The receiver side analysis can be divided into two main parts which are the Received Hologram Analysis and Reconstructed Object Image Analysis.

1. Received Hologram Analysis

At the receiver, transmitted holograms remained intact, ensuring secure CGH communication. Using demuxed reference waves, magnitude and phase were separated, and reconstructed images were recovered as shown in Figure 18.

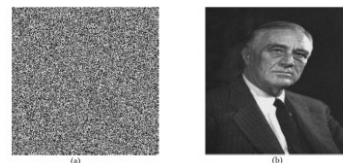


Figure 18. (a) Received Hologram, (b) Reconstructed transmitted image.

2. Reconstructed Object Image Analysis

The Reconstructed Object Image Analysis includes two sections: Operating wavelength analysis for reconstructed color object image and Fresnel distance analysis for reconstructed gray object image. However, wavelength analysis in Figure 19 shows that advanced Fresnel CGH performs best in the visible spectrum (390–700 nm). At $\lambda_1=350$ nm, $\lambda_2=470$ nm (Figure 19 (a)), images were sharp and blur-free, while $\lambda_1=630$ nm, $\lambda_2=700$ nm (Figure 19 (b)) enhanced contrast and sharpness. Communication wavelengths (e.g., 1500 nm) made images invisible. On the other hand, in Fresnel CGH, the Fresnel distance affects image quality. At $z_1=12$ cm (Figure 20 (a)), images had minimal ringing and blurring. At $z_1=7$ cm (Figure 20 (b)), improvements were limited, and at $z_1=1$ cm (Figure 20 (c)), quality degraded. At $z_1=0.1$ cm (Figure 20 (d)), distortion worsened. So, it can be said that larger Fresnel distances improve reconstruction.

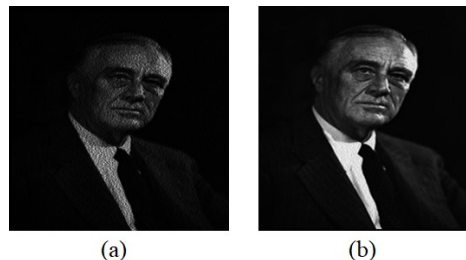


Figure 19. (a) Reconstructed image ($\lambda_1=350$ nm, $\lambda_2=470$ nm), (b) Reconstructed image ($\lambda_1=630$ nm, $\lambda_2=700$ nm).

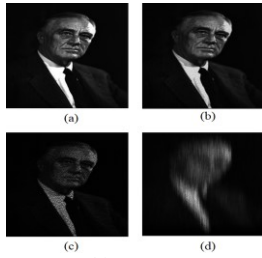


Figure 20. (a) Reconstructed image ($z_1=12\text{cm}$), (b) Reconstructed image ($z_1=7\text{cm}$), (c) Reconstructed image ($z_1=1\text{cm}$), (d) Reconstructed image ($z_1=0.1\text{cm}$).

Performance Analysis of Advanced Fresnel Algorithm

The performance of the Advanced Fresnel Algorithm is measured using parameters like RGB Color Space, Histogram, Correlation Coefficient, and Entropy. Among these, RGB Color Space Analysis is the best because it directly evaluates the color quality and preservation in the reconstructed image, making it crucial for assessing visual fidelity.

Reconstructed RGB images were analyzed for hue, saturation, contrast, and brightness. The red band showed low values of Figure 21, while green was well-recovered with balanced properties of Figure 22. The blue band lacked green hue and saturation, with low brightness and overlapping contrast of Figure 23. Effective recovery was achieved for green and blue, but red data remained limited.



Figure 21. (a) Transmitted red band image, (b) Reconstructed red band image.

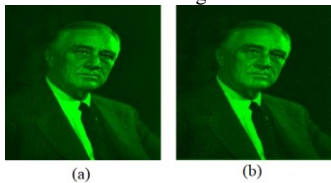


Figure 22. (a) Transmitted green band image, (b) Reconstructed green band image.



Figure 23. (a) Transmitted blue band image, (b) Reconstructed blue band image.

iv) Comparison Among Three Advanced CGH Methods

This study compares Fraunhofer, GS, and Advanced Fresnel diffraction Algorithms. Fraunhofer faces 'twin-image' issues, GS may distort phases, while Advanced Fresnel effectively reconstructs near-field holograms. Evaluations use RMSE, contrast, entropy, and pixel correlation metrics.

Root Mean Square Error (RMSE) Analysis

Figure 24 shows the RMSE of reconstructed image for three different methods in a graphical representation. Here, GS algorithm method shows the lowest RMSE and Fresnel diffraction method shows the largest error.

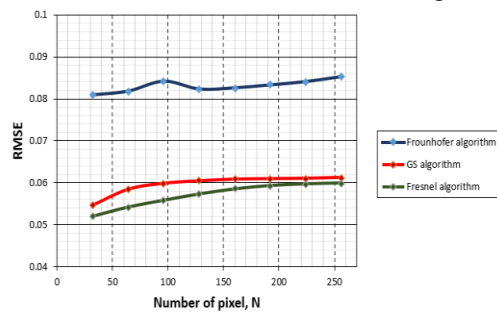


Figure 24. RMSE with respect to the number of pixels using different algorithms.

Contrast Analysis

The contrast performance analysis of the three algorithms can be depicted in Figure 25. It can be seen that the GS algorithm's iterative process, influenced by pixel count and iteration number, limits its practicality. Moreover, Fresnel and Fraunhofer methods offer better stability and contrast, with higher iterations enhancing image quality.

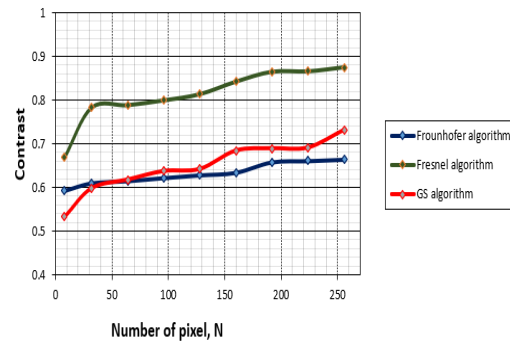


Figure 25. Contrast of reconstructed image with respect to the number of pixels of using different algorithms.

Entropy and Redundancy Analysis

Entropy in holographic algorithms measures information content, while redundancy reflects data duplication. Redundancy can be measured by Eq. (24).

$$Redundancy = H_{max} - H \quad (24)$$

Table 3 highlights the Fresnel algorithm's superior entropy and lower redundancy compared to GS and Fraunhofer, offering better security and resistance to statistical attacks.

Table 3. Entropy and Redundancy values.

| <i>Entropy and Redundancy values</i> | | | |
|--------------------------------------|-----------------------|----------|-------------------|
| <i>Algorithm</i> | <i>Entropy, H</i> | | <i>Redundancy</i> |
| | Original object image | Hologram | |
| Fraunhofer | 4.6326 | 7.4232 | 0.5768 |
| GS | 3.1980 | 7.9880 | 0.0120 |
| Fresnel | 6.5326 | 7.9895 | 0.0105 |

Histogram Analysis

Histogram of Fresnel algorithm (a) object image, (b) hologram; Histogram of GS algorithm (c) object image, (d) hologram; Histogram of Fraunhofer algorithm (e) object image, (f) hologram have been depicted in Figure 26. It suggests that compared to GS and Fraunhofer algorithms, the Fresnel algorithm offers a more uniform distribution of pixels.

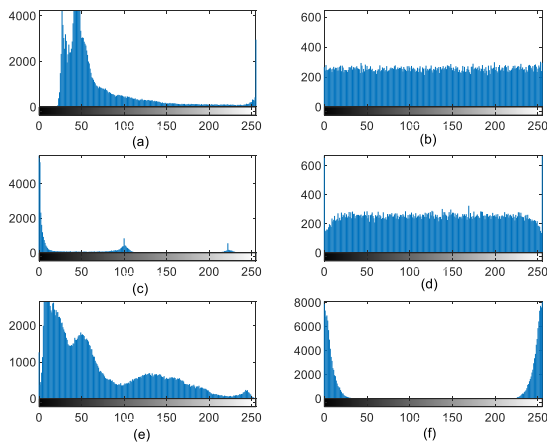


Figure 26. Histogram of Fresnel algorithm (a) object image, (b) hologram; Histogram of GS algorithm (c) object image, (d) hologram; Histogram of Fraunhofer algorithm (e) object image, (f) hologram.

Correlation of Adjacent Pixels Analysis

This study assesses security using Adjacent Pixels' Correlation Coefficient (APCC). Effective algorithms achieve APCC values near zero, reducing horizontal and vertical pixel correlations to ensure image security.

Table 4. Summary Comparison of Performance Parameters for Three Holographic Algorithms

| Parameter | Fraunhofer Algorithm | GS Algorithm | Advanced Fresnel Algorithm |
|----------------------------------|--|---|---|
| Histogram Analysis | Moderate uniformity in pixel distribution, some identifiable patterns. | Low uniformity due to phase mask, some pattern artifacts. | High uniformity, minimal identifiable patterns, resistant to statistical attacks. |
| Correlation Coefficient Analysis | Moderate APCC values, indicating partial correlation in adjacent pixels. | Slightly lower APCC than Fraunhofer, showing improved decorrelation. | Significantly low APCC, suggesting strong decorrelation and enhanced security. |
| Entropy Analysis | Moderate APCC values, indicating partial correlation in adjacent pixels. | Entropy ~7.9880 for holograms; minimal redundancy but moderate information retention. | Entropy ~7.9895 for holograms; high information retention and minimal redundancy. |

Table 5. Summary Findings of Three Holographic Algorithms for Different References

| Performance Parameters | Summary of Findings | References |
|----------------------------------|--|-----------------------------|
| Histogram Analysis | Demonstrated significant improvements in image clarity with histogram equalization techniques. | [6], [8], [20], [14], [16] |
| Correlation Coefficient Analysis | Achieved high correlation coefficients indicating robust pattern recognition. | [18], [6], [15], [17], [10] |
| Entropy Analysis | High entropy values suggest a diverse representation of data. | [13], [12], [11], [4], [7] |

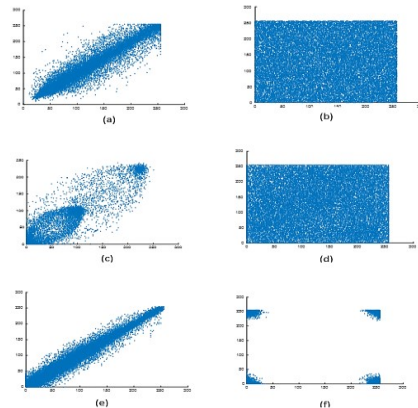


Figure 27. Correlation of Fresnel algorithm (a) object image, (b) hologram; GS algorithm correlation (c) object image, (d) hologram; Fraunhofer algorithm correlation (e) object image, (f) hologram.

Figure 27 shows the advanced Fresnel algorithm performing slightly better than Fraunhofer and GS algorithms. Summary performance comparisons and findings for the three algorithms are presented in Table 4 and 5.

Our CGH system encrypts images into multiplexed holograms via WDM, ensuring high security, efficiency, and tamper resistance, surpassing traditional methods in data rates and parallel processing for secure optical communication.

4. Conclusion

This research developed a secure communication system using three algorithms: Fraunhofer diffraction, Gerchberg-Saxton (GS), and advanced Fresnel diffraction. While Fraunhofer faced limitations with twin images, the GS algorithm effectively reconstructed 3D objects. The advanced Fresnel method excelled in contrast and entropy, making it the preferred choice. An improved Fresnel-based CGH calculation program enhanced protective hologram complexity while ensuring system compatibility. Future research could explore applications in holographic storage, authentication, navigation, and interactive displays, integrating technologies such as facial recognition and fingerprint detection to drive practical advancements in holography.

References

- [1] C. Slinger, C. Cameron and M. Stanley, "Computer-generated holography as a generic display technology," *Computer*, vol. 38, no. 8, pp. 46 - 53, 08 August 2005.
- [2] Ferdous Ahmed and Md. Sultan Mahmud, "Fourier Optics and Computer Generated Hologram," *International Journal of Computational Science and Engineering*, vol. 5, no. 1, pp. 1-7, 2015.
- [3] Gülhan Ustabas Kaya, Ali Dursun, Zehra Saraç, "A novel reconstruction method using the Phase only information of the Computer Generated Hologram," *International Conference on Advances In Computer and Electronics Technology - ACET 2013*, vol. 32, no. 3, pp. 17 - 20, 2013.
- [4] Edward Buckley, "Holographic Laser Projection," *Journal of Display Technology*, vol. 7, no. 3, pp. 135-140, 2011.
- [5] Martin J. Richardson, John D. Wiltshire, *Conventional Holography and Lasers*, 1 ed., Wiley-IEEE Press, 2018, pp. 55 - 75.
- [6] Min Liu, Guanglin Yang, "Improved reconstruction for computer-generated hologram from digital images," *Asia-Pacific Signal and Information Processing Association Annual Summit and Conference*, pp. 1-4, 2013.
- [7] Alicia V. Carpentier, Humberto Michinel and José R. Salgueiro, "Making optical vortices with computer-generated holograms," *American Journal of Physics*, vol. 76, no. 10, pp. 61-67, October 2008.
- [8] D. D. W. Olson, "The elementary plane-wave model for hologram ray tracing," *American journal of physics*, vol. 57, no. 5, 1989.
- [9] Adam Overvig, Sajan Shrestha, Changxi Zheng and Nanfang Yu, "High-efficiency amplitude-phase modulation holograms based on dielectric metasurfaces," *Conference on Lasers and Electro-Optics (CLEO)*, pp. 1-2, May 2017.
- [10] Liu Shou, Wang Jin-Cheng, Hsu Da-Hsiung, "The art and science of anti-counterfeit embossed rainbow holograms," *Third International Conference on Holographic Systems, Components and Applications*, pp. 210-212, 1991.
- [11] Martin J. Richardson, John D. Wiltshire, *Making Conventional Denisyuk, Transmission and Reflection Holograms in the Studio*, 1 ed., Wiley-IEEE Press, 2018, pp. 185-238.
- [12] A. W. Lohmann and B. R. Brown, "Complex Spatial Filtering with Binary Masks," *Applied Optics*, vol. 5, no. 6, p. 967, 1966.
- [13] L. B. Lesem, P. M. Hirsch, J. A. Jordan, "The Kinoform: A New Wavefront Reconstruction Device," *IBM Journal of Research and Development*, vol. 13, no. 2, pp. 150 - 155, March 1969.
- [14] M. R. Hossain, A. Haque, O. Mojumder, F. Akter, "A Novel Implementation of Computer Generated Hologram for Highly Secured Communication Using Gerchberg-Saxton (GS) Algorithm," *IEEE Region 10 Symposium (TENSYP)*, pp. 1286-1289, June 2020.
- [15] Wang, Z.; Li, Y.; Tang, Z.; Li, Z.; Wang, D. Fast Hologram Calculation Method Based on Wavefront Precise Diffraction. *Micromachines* 2023, 14, 1690.
- [16] Su, P., Cao, W., Ma, J., Cheng, B., Liang, X., Cao, L. and Jin, G., 2016. Fast computer-generated hologram generation method for three-dimensional point cloud model. *Journal of Display Technology*, 12(12), pp.1688-1694.
- [17] Pang, H., Wang, J., Cao, A., Zhang, M., Shi, L. and Deng, Q., 2016. Accurate hologram generation using layer-based method and iterative Fourier transform algorithm. *IEEE Photonics Journal*, 9(1), pp.1-8.
- [18] Minikhanov, T.Z., Zlokazov, E.Y., Cheremkhin, P.A., Starikov, R.S. and Evtikhiev, N.N., 2023. Computer-Generated Holography Methods for Data Page Reconstruction Using Phase-Only Medium. *Applied Sciences*, 13(7), p.4479.